Geophysical Journal International

Geophys. J. Int. (2012) **188,** 891–907 doi: 10.1111/j.1365-246X.2011.05281.x

The satellite along-track analysis in planetary magnetism

Erwan Thébault,[1] Fotini Vervelidou,[1] Vincent Lesur[2] and Mohamed Hamoudi[2]

[1]*Equipe de géomagnétisme, Institut de physique du globe de Paris - Sorbonne Paris Cité, UMR CNRS* 7154, *Université Paris Diderot,* 1 *rue Jussieu,* 75005 *Paris, France. E-mail: ethebault@ipgp.fr*

[2]*Helmholtz Centre Potsdam, GFZ German Research Centre for Geosciences, Telegrafenberg* 14473, *Germany*

Accepted 2011 October 22. Received 2011 September 8; in original form 2011 February 15

SUMMARY

Many physical characteristics of planets, such as their topography, magnetic and gravitational fields, are routinely detected and measured by spacecrafts. At satellite altitudes, even if little is known about the measured signal, it is possible to separate the large-scale components from other contributions by a spectral analysis carried out along the spacecraft orbit. This procedure, which dates back to the early age of the satellite era, is routinely applied with spherical harmonics analysis for the study of large-scale planetary magnetic fields, particularly those that vary rapidly in time. In this paper, we review the approximations of this procedure for investigating internal and external magnetic fields of planets. We show that the magnetic field analyses along the orbits are limited by a finite frequency resolution that is known to introduce a spectral leakage. This leakage may lead to artificial spatio-temporal variations of the magnetic field, such as an apparent internal field secular variation, an asymmetry of the magnetospheric field and a regional distortion of the lithospheric field structures. We quantify the errors for the Earth's lithospheric field and display its distribution in the spatial and the spectral domains. We also discuss these limits for the Moon and Mars lithospheric magnetic fields. Our analytical results illustrate the pros and cons of the orbit-by-orbit analyses and should allow us to avoid the pitfall of geophysical overinterpretation of some artificial magnetic field variations.

Key words: Fourier analysis; Spatial analysis; Magnetic anomalies: modelling and interpretation; Satellite magnetics.

1 INTRODUCTION

Satellite missions continue to provide crucial measurements of the physical properties of the Earth and other planets in our solar system. Representing these satellite measurements with appropriate models and basis functions is an important procedure for imaging problems and geophysical inference. For this reason, geophysics and the space sciences call for a large class of techniques related to spectral and data analysis, inverse problems and interpolation of measurements. In a wide range of applications, the mathematical solution of a problem is expressed in terms of an infinite series of basis functions that gives rise to mathematically ill-posed problems (because the number of data will always be finite whereas the number of parameters is theoretically infinite). A way to circumvent this difficulty is to sample the model space by truncating the series expansion or by selecting empirically what is thought to be the most relevant subset of terms. Unfortunately, the reduction of the model space is known to introduce an undesirable effect in the solution known as spectral leakage. The spectral leakage is the conversion of the energy normally carried by a term of the infinite series that was excluded from the solution into another one that belongs to truncated model selected *a priori* (Trampert & Snieder 1996 for a discussion in tomography).

Magnetic fields emanating from a planet are no exception as their mathematical solutions are often expressed in terms of an infinite series of spherical harmonics (SH). In addition, magnetic fields have a large variety of sources whose contributions overlap in space and in time (Langlais *et al.* 2009). The proper separation of the total signal into its individual constituents and the selection of the most relevant subset of SH is, in general, a very challenging problem. The spectral leakage is unavoidable but its prominence depends greatly on the technique applied to model the magnetic field measurements.

In space, magnetic measurements are acquired with magnetometers embarked aboard spacecrafts. Two procedures are then commonly employed to analyse the measurements and separate the source fields. The first one, referred to as 'comprehensive', determines all known magnetic field contributions through a grand inversion (e.g. Sabaka *et al.* 2004). It requires hypotheses about the origin and the geometry of the different sources to parametrize the solution and to select the most relevant subset of basis functions. When the parametrization error is small, the spectral leakage is negligible. Otherwise, we find that the model output strongly depends on the chosen parametrization. When little

a priori knowledge or measurements of the planetary magnetic field are available to guide the model parametrization, an effective technique called sequential analysis can be used. It requires a careful visual inspection of the data in which each source contributing to the total magnetic field is individually and empirically identified and then subtracted from the measurements. Some fundamental differences between the comprehensive and the sequential approaches, in particular, with respect to the predicted magnetic field power spectrum, are discussed in Sabaka & Olsen (2006). Here, we restrict ourselves to the study of one aspect of the sequential modelling, which consists in analysing the field along a portion of the satellite orbits. This situation often arises in planetary exploration when the magnetic field environment changes from one satellite orbit to another so that the parameter value varies rapidly in time.

The magnetometer data analysis along satellite orbits was applied on the Polar Orbital Geophysical Observatory (POGO; 1965–1971) measurements (Cain 2007), allowing scientists to realize the strong influence and time variability of the Earth's external magnetic field (Langel & Sweeney 1971). Since then, the technique was used to process the MAGSAT (1979–1980; Langel *et al.* 1982; Langel & Estes 1985; Cohen & Achache 1990, 1994; Arkani-Hamed *et al.* 1994; Ravat *et al.* 1995), Oersted (1999–; Neubert *et al.* 2001) and CHAMP (2000–2010; Reigber *et al.* 2000) satellite data (Maus *et al.* 2002). For the Earth, an overview of the achievements made possible thanks to satellite along-track analyses is given by Langel & Hinze (1998, chap. 4.4). Planetary investigations also rely extensively upon data measured along flybys that often provide the only quantitative knowledge about a magnetic field. The technique was applied during the Mariner 10 (1974–1975) spacecraft mission (Ness *et al.* 1974) and more recently on the MESSENGER's data measured during its three flybys around Mercury (Purucker *et al.* 2009; Uno *et al.* 2009). In many other situations, for instance unveiling the Lunar crustal field, it remains an efficient empirical tool to correct the measurements for the influence of the Earth and solar magnetic fields (Hood *et al.* 2001; Purucker & Nicholas 2010).

The along-track analysis of satellite data has some merits. From a practical viewpoint, it is easy to apply and provides a useful first-order solution to possibly complicated problems. Nonetheless, when high accuracy and resolution are sought and made possible by the measurements, the along-track analysis is deficient to an extent that still needs to be defined. Several questions were raised in the past, most of them in the context of mapping the Earth's crustal magnetic field. Singh *et al.* (1986) wondered if part of the internal field signal could not seep into the external field component after along-track analyses, causing a deletion of the crustal field in the large wavelengths range (Ravat *et al.* 1995; Purucker *et al.* 1997). Cohen and Achache (1994) noted a reduced amplitude of the predicted magnetic field in the direction of the MAGSAT satellite orbit and wondered if the analysis along the satellite orbits could cause model anisotropy, like a loss of north–south signal over large cretaceous quiet zones in the oceanic domain (Grammatika & Dyment 1997). Other authors have suggested that it could transport signal from oceans onto the land areas and therefore lead to spurious local magnetic field features (Tyler *et al.* 2003) and cause artificially reduced SH predicted power spectra (Hemant & Maus 2003; Sabaka & Olsen 2006); a drawback important for geological interpretation in terms of magnetization or magnetic crustal thickness. More recently, Purucker & Whaler (2007, p. 225) further inquired whether the along-track filtering could prevent separating the induced from the remnant magnetization in the Earth's crust. The list of possible drawbacks if therefore substantial but it is difficult to identify and to quantify the errors from these works. The aim of this paper is to better define the limits of this technique to quantify the level of spectral leakage that is introduced by the analysis of a planetary magnetic field along some portion of a satellite orbit (along-track analysis). This work was prompted by the recent successful planetary spatial programs (Solomon *et al.* 2008) and the planned Earth's multisatellites Swarm mission (Friis-Christensen *et al.* 2006) that will require accurate processing to exploit fully the quality of their measurements. Each planetary satellite mission represents a particular case for which the efficiency of an along-track analysis depends on data availability and distribution and has to be evaluated by numerical simulations. Here we attempt to address the problem in a formal way to stay as general as possible although we have to restrict ourselves to an ideal case (a satellite moving along a circular polar orbit) that we mathematically describe in the first section. This case allows us to put a natural emphasis on the Earth, whose data coverage and quality are by far the best and the most comprehensive. We then study the limitations of the along-track analysis for the identification of large-scale internal and external magnetic fields. In a third part, we finally discuss the problems raised by the along-track analysis when these large-scale magnetic field estimates are used as a data correction with the purpose of discovering the smaller lithospheric field structures.

2 DEFINITIONS AND HYPOTHESES OF THE ALONG-TRACK ANALYSIS

The satellite along-track analysis can be performed with a large variety of mathematical functions that do not always have well-founded physical justification for geomagnetism. This analysis can be based on geographic polynomials, splines, wavelets or high-pass filters, etc. (Langel & Hinze 1998, chap. 4.4 for a review). We do not discuss these approaches but refer to Wang (1987) for an overview of the issues raised by Fourier analysis along circular profiles. We focus instead on the SH analysis along the satellite orbits because it is apparently physically convincing for global studies of a planetary magnetic field outside the sources. Separating the internal and the external magnetic fields from a discrete set of measurements requires some prior knowledge about the magnetic field sources. In practice, we assume that the interplanetary magnetic field (which varies with time) and its interaction with a magnetosphere, when the planet generates an internal global magnetic field, is large scale. This widely accepted assumption is reasonable on Earth but the supremacy of the crustal magnetic field on Mars (Langlais *et al.* 2004) illustrates the possible weakness of this paradigm for other planets.

We keep the same approximations and we assume that the main internal and external fields can be described with a low degree SH along a large portion of a satellite path. We discard the case of scalar measurements that does not allow us to derive linear equations and we assume that the calculation is performed in a source-free region. Because the scalar magnetic potential V obeys the Laplace equation $\nabla^2 V = 0$, it

may be expressed in a spherical coordinate system in terms of an infinite series

$$V = a\sum_{n=1}^{\infty}\sum_{m=0}^{n}\left\{\left[g_n^m(t)\cos(m\varphi)+h_n^m(t)\sin(m\varphi)\right]\left(\frac{a}{r}\right)^{n+1}+\left[q_n^m(t)\cos(m\varphi)+s_n^m(t)\sin(m\varphi)\right]\left(\frac{r}{a}\right)^{n}\right\}P_n^m(\cos\theta), \tag{1}$$

with $P_n^m(\cos\theta)$ the associated Legendre functions of degree n and order m (in the following we write $P_n^m(\theta)$ or simply P_n^m for the purpose of brevity) with r, φ and θ, the radial distance, the longitude and the colatitude in the planet's reference frame, a the reference radius and t the time. The total vector magnetic field $\mathbf{B} = B_r\mathbf{u}_r + B_\theta\mathbf{u}_\theta + B_\varphi\mathbf{u}_\varphi$ (with the unit vectors $\mathbf{u}_r$, $\mathbf{u}_\theta$, $\mathbf{u}_\varphi$ pointing radially upwards, southwards and eastwards) is the linear superimposition of the internal and external contributions

$$\mathbf{B}(t) = \mathbf{B}^m(t)+\mathbf{B}^e(t)+\mathbf{B}^c, \tag{2}$$

where $\mathbf{B}^m(t)$, $\mathbf{B}^e(t)$ and $\mathbf{B}^c$ are the main, external and crustal fields. Each of the three components $(B_r, B_\theta, B_\varphi)$ is obtained by setting $\mathbf{B}(t) = -\nabla V(t)$. We postulate that the magnetic field is perfectly described by the sets of internal $\{g_n^m, h_n^m\}$ and external $\{q_n^m, s_n^m\}$ Gauss coefficients (up to a maximum SH degree that will be defined in due course). More complicated source distribution are not considered here and the external field $\mathbf{B}^e$ is assumed to be external to the satellite orbit, static over an entire half-orbit and, together with $\mathbf{B}^m$, larger scale than the static internal crustal field $\mathbf{B}^c$.

We choose polar satellite orbits because not only it corresponds to an idealized version of the quasi-polar Earth's satellite missions, but also it simplifies the handling of the orthogonality properties of the associated Legendre functions. Let us consider the dipole and quadrupole parts of the zonal magnetic field (order $m = 0$) that are symmetric with respect to the axis of revolution in the planetary reference frame, and let us define by $\widetilde{\mathbf{B}}^0$ the internal and external symmetric fields that are to be estimated along some portion of the orbit. Because this field is assumed to be large scale we expand it in SH to degree $n = 2$ only (we could in principle expand it to a higher degree)

$$\widetilde{B}_r^0 = \sum_{w=1}^{2}\left\{(w+1)\widetilde{g}_w^0\left(\frac{a}{r}\right)^{w+2} - w\widetilde{q}_w^0\left(\frac{r}{a}\right)^{w-1}\right\}P_w^0(\theta), \tag{3}$$

$$\widetilde{B}_\theta^0 = -\sum_{w=1}^{2}\left\{\widetilde{g}_w^0\left(\frac{a}{r}\right)^{w+2} + \widetilde{q}_w^0\left(\frac{r}{a}\right)^{w-1}\right\}\frac{\mathrm{d}P_w^0(\theta)}{\mathrm{d}\theta}, \tag{4}$$

$$\widetilde{B}_\varphi^0 = 0, \tag{5}$$

with $\widetilde{q}_w^0$ and $\widetilde{g}_w^0$ the external and internal estimates of the true Gauss coefficients q_w^0 and g_w^0. Eqs (3), (4) and (5) are particularly useful when one wants to verify the existence of the dipole field and to estimate its dominance over other terms when only a few spacecraft orbits or flybys are available (Ness *et al.* 1974). If we subtract the dominant main field $\mathbf{B}^m$ in eq. (2) and neglect the crustal field $\mathbf{B}^c$, then $\widetilde{\mathbf{B}}^0$ is an estimate of the external field $\mathbf{B}^{0e}$. Therefore, the linear inversion of eq. (3) in a least-squares sense, given in practice a set of discrete magnetic field measurements, provides a simple way to estimate the coefficients $\widetilde{q}_w^0$ and $\widetilde{g}_w^0$ and therefore to describe mathematically the symmetric magnetospheric field (the so-called ring current) and its counterpart induced in the Earth's mantle. The estimated coefficients can then be used to correct the magnetic data for the magnetospheric field (Maus *et al.* 2002) and to give us access to the crustal field $\mathbf{B}^c$ (eq. 2), or to establish time-series for inferring mantle conductivities (Balasis *et al.* 2004). For a more realistic comparison with the Earth's magnetospheric field this equation should be expressed in the geomagnetic reference frame but our treatment does not require this subtlety.

Formally, the inverse problem in the least-squares sense can be solved along a half-orbit (one satellite 'track') by assuming that the satellite travels from one geographic pole to another and provide continuous measurements. Therefore, the coefficients $\widetilde{g}_w^0$ and $\widetilde{q}_w^0$ minimize the cost function $\chi^2 = \int_0^\pi \left(\mathbf{B}-\widetilde{\mathbf{B}}^0\right)^2\sin\theta\mathrm{d}\theta$. Their formal expressions become

$$\widetilde{q}_w^0 = \frac{1}{2w+1}\sum_{n=1}^{\infty}\sum_{m=0}^{n}\left[\beta_{w,n}^m(w+1)\left\{\iota_n^m(\varphi)\left(\frac{a}{r}\right)^{n+w+1}+\varepsilon_n^m(\varphi)\left(\frac{r}{a}\right)^{n-w}\right\}+\gamma_{w,n}^m\left\{n\varepsilon_n^m(\varphi)\left(\frac{r}{a}\right)^{n-w}-(n+1)\iota_n^m(\varphi)\left(\frac{a}{r}\right)^{n+w+1}\right\}\right], \tag{6}$$

$$\widetilde{g}_w^0 = \frac{1}{2w+1}\sum_{n=1}^{\infty}\sum_{m=0}^{n}\left[\beta_{w,n}^m w\left\{\iota_n^m(\varphi)\left(\frac{a}{r}\right)^{n-w}+\varepsilon_n^m(\varphi)\left(\frac{r}{a}\right)^{n+w+1}\right\}+\gamma_{w,n}^m\left\{(n+1)\iota_n^m(\varphi)\left(\frac{a}{r}\right)^{n-w}-n\varepsilon_n^m(\varphi)\left(\frac{r}{a}\right)^{w+n+1}\right\}\right], \tag{7}$$

with

$$\gamma_{w,n}^m = \frac{\left\langle P_w^0, P_n^m\right\rangle}{\left\|P_w^0\right\|^2} \tag{8}$$

and

$$\beta_{w,n}^m = \frac{\left\langle \frac{\mathrm{d}P_w^0}{\mathrm{d}\theta}, \frac{\mathrm{d}P_n^m}{\mathrm{d}\theta}\right\rangle}{\left\|\frac{\mathrm{d}P_w^0}{\mathrm{d}\theta}\right\|^2}, \tag{9}$$

with

$$\iota_n^m(\varphi) = g_n^m\cos(m\varphi)+h_n^m\sin(m\varphi) \tag{10}$$

and

$$\varepsilon_n^m(\varphi) = q_n^m\cos(m\varphi)+s_n^m\sin(m\varphi), \tag{11}$$

where $\langle f, g\rangle = \int_0^\pi fg \sin\theta \mathrm{d}\theta$, $\|f\|^2 = \int_0^\pi f^2 \sin\theta \mathrm{d}\theta$, and $w = 1, 2$. Note that the numerical value of the dot products depends on the parity of the triplet n, w and m with, in particular, $\gamma^m_{w,n} = \beta^m_{w,n} = 0$ for $n + m + w$ odd (Ashour 1964). Moreover, the dot products are defined with respect to the weight $\sin\theta$, which does not correspond to the reality of raw measurements that are evenly spaced. This shows that in practice the data analysed along the orbits must be weighted by $\sin\theta$ to preserve numerically the orthogonality properties of the Legendre functions. For the purpose of discussion, we keep the formulae written explicitly in function of $\iota^m_n(\varphi)$ and $\varepsilon^m_n(\varphi)$ that contain respectively the internal and external Gauss coefficients that describe the total vector magnetic field (eqs 10 and 11).

3 MAGNETIC FIELD ANALYSES ALONG SINGLE ORBITS

Eqs (6) and (7) show that the estimation of the symmetric field depends on the path of the satellite. In practice, when planetary magnetic measurements are analysed in SH, the discussion is often focused on the conditioning of the inverse problems. A poor conditioning leads to numerical difficulties but also helps to evaluate the robustness of the estimated parameters (Russel & Dougherty 2009). In addition to this technical problem, we see here that the Gauss coefficients $\{\widetilde{g}^0_w, \widetilde{q}^0_w\}$ can be perfectly well determined in a least-squares sense but nonetheless be linearly correlated with the magnetic field signal over the longitude of the meridian. We may obtain a robust numerical estimation of the parameters but we cannot avoid the spectral leakage of the magnetic field structures present along the orbit into the solution; the estimated parameters do not covary but are biased. Therefore, the posterior parameter error estimated by an inverse problem may be misleading because it may severely underestimate the true error depending on the level of contamination of all other source fields. From eqs (6) and (7) we see that two satellite paths at different longitudes but identical altitudes may create a wrong impression of axial asymmetry of the external field whereas two paths at the same longitude but different altitudes may introduce an impression of time variation. It then becomes difficult to judge the validity of the SH solution when the solution is obtained along elliptic and inclined orbits. Nowadays, satellites probing the Earth and measuring the magnetic field travel along quasi-circular orbits but in planetary exploration elliptical orbits are common (Connerney 2009); MESSENGER being one of the latest mission in elliptical mapping orbit (MO). Scientists involved in the data representation are generally aware of these problems but the bias, which can be roughly estimated by eqs (6) and (7) under some assumption on the magnetic field power spectrum, is rarely quantified.

Let us illustrate these consequences for the first-order study of a magnetic field external to a satellite orbit. We assume temporarily that the 'true' external field is dipolar and zonal (therefore, $\varepsilon^m_n(\varphi) = q^0_1$ for $n = 1$, $m = 0$ and $\varepsilon^m_n(\varphi) = 0$ otherwise) and that some weak contributions of the internal field (main or crustal) are present ($\iota^m_n(\varphi) \neq 0$). In this case, $\widetilde{\mathbf{B}}^0$ is an estimation of the symmetric magnetospheric field $\mathbf{B}^{0e}$. Expressions (6) and (7) reduce, respectively, to

$$\widetilde{q}^0_w = q^0_w + \frac{1}{2w+1}\sum_{n=1}^{\infty}\sum_{m=0}^{n}\iota^m_n(\varphi)\left(\frac{a}{r}\right)^{n+w+1}\left\{(w+1)\beta^m_{w,n} - (n+1)\gamma^m_{w,n}\right\}, \tag{12}$$

$$\widetilde{g}^0_w = \frac{1}{2w+1}\sum_{n=1}^{\infty}\sum_{m=0}^{n}\iota^m_n(\varphi)\left(\frac{a}{r}\right)^{n-w}\left\{w\beta^m_{w,n} + (n+1)\gamma^m_{w,n}\right\}. \tag{13}$$

Eq. (12) shows that $\widetilde{q}^0_w$ varies in longitude around the true value q^0_w if $\iota^m_n(\varphi) \neq 0$, while the estimated $\widetilde{\mathbf{B}}^{0e}$ should be axisymmetric. As was expected, there is a leakage of the internal field components into the external field coefficients $\widetilde{q}^0_w$. In a more realistic situation where $\varepsilon^m_n(\varphi)$ is not purely dipolar and varies in time (as a result of differing solar wind and interplanetary magnetic field conditions between orbits), the coefficients $\widetilde{q}^0_w$ and $\widetilde{g}^0_w$ would become too tightly intertwined to identify reliably $\widetilde{g}^0_w$ as being the internal 'induced' counterpart of $\widetilde{q}^0_w$. This, in turn, could lead to difficulties in computing planetary upper mantle conductivities at high frequencies (Olsen 1999). The relative accuracy of $\widetilde{q}^0_w$ with respect to the true q^0_w increases when the external contributions $\varepsilon^m_n(\varphi)$ are comparatively larger than the internal ones $\iota^m_n(\varphi)$. Therefore, the magnetic field of the ring current, mathematically represented by $\widetilde{q}^0_w$, is proportionately better estimated during high level of external field activity; a situation we often seek to avoid by selecting data at magnetically quiet times unless, of course, the purpose is to study the ring current during magnetic storm times. These latter conclusions address well some of the questions raised by Regan *et al.* (1981) when processing the scalar POGO real measurements.

We now consider three simplistic numerical examples calculated at 400 km altitude above a non-rotating Earth with a mean radius $a = 6371.2$ km. The values for g^0_1 and q^0_1 of the external field $\mathbf{B}^{0e}$ (eqs 12 and 13) are chosen for magnetic quiet times as (Langel & Estes 1985)

$$q^0_1 = 19.45 - 0.66Dst, \tag{14}$$

and

$$g^0_1 = -6.1 + 0.27q^0_1. \tag{15}$$

The disturbance storm-time Dst is a proxy measuring the symmetric magnetospheric field calculated on Earth using ground based magnetic observatory measurements (Sugiura 1964). We set arbitrarily $Dst = -15$ nT, which corresponds to the mean Dst value between years 2000 and 2010.

For case 1, we assume that external field is symmetric ($\mathbf{B}^e = \mathbf{B}^{0e}$) and that none of the internal field contributions were corrected for ($\mathbf{B}^m \neq \mathbf{0}$, $\mathbf{B}^c \neq \mathbf{0}$). The expression of $\iota^m_n(\varphi)$ in eq. (10) is calculated with the CM4 Gauss coefficients at epoch 2001.0 to SH degree 65 for the

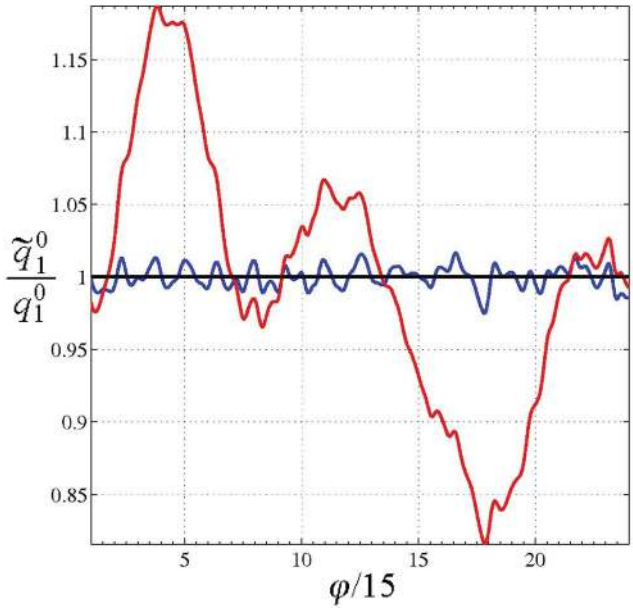

Figure 1. We display the ratio between the $\widetilde{q}_1^0$ estimated along a satellite circular half-orbit and the initial q_1^0 external Gauss coefficient assuming that other sources than external field may contribute to the vector magnetic field along the satellite pole-to-pole path. The black curve is obtained when a symmetric external fields is considered; the blue curve is obtained when a symmetric external plus a crustal field model are contributing to the total vector field; the red curve is obtained when a symmetric external field, a crustal field, and the difference between the GRIMM2 (Lesur *et al.* 2010) main field models for epochs 2005.5 and 2006 contribute to the field along the synthetic orbit.

internal main and crustal fields (Sabaka *et al.* 2004). We then estimate $\widetilde{q}_i^0$ using eq. (12). In this example (not illustrated), the estimation of $\widetilde{q}_1^0$ fails entirely because the main field dipole coefficient g_1^0 carries most of the Earth's total field [$\iota_1^0(\varphi) \gg \varepsilon_1^0(\varphi)$].

For case 2, the $\iota_n^m(\varphi)$ contains the internal main field difference between epochs 2005.5 and 2006 of the GRIMM2 model (Lesur *et al.* 2010) for SH degree 1–14 and the CM4 crustal field from degree 15 to 65. This example mimics a main field correction with an error of 6 months (like an error in representing the secular variation); a typical case we meet in practice when the data are corrected for an imperfect main field model centred on epochs different from the data epochs, like an International Geomagnetic Reference Field model (Finlay *et al.* 2010). This example shows that the main field residuals create an artefact in the estimate $\widetilde{q}_1^0$ (Fig. 1) that depends on the longitude. In local time (LT), this may lead to flawed interpretations in terms of asymmetry of the magnetospheric field. The relative error between q_1^0 and $\widetilde{q}_1^0$ (Fig. 1) is well represented by a function with a periodicity of 8 and 24 hr (assuming that for a static Earth the LT is comparable to $\varphi/15$). Although difficult to expand to a real satellite configuration, this is reminiscent of a relationship established by Langel & Estes (1985) between the coefficient q_1^0 and the LT. We cannot challenge their result on the basis of Fig. (1) only but we illustrate its striking similarity with an apparent LT variation caused by the leakage of the internal field (in this case, 6 months of secular variation). We also note that it was obtained with scalar POGO magnetic field measurement along elliptical orbits with a main field correction involving a linear prediction in time of the secular variation. Such data type, distribution and model correction represent an unfavourable situation that, according to eq. (12), could introduce a significant error.

For case 3, we assume a zonal external field (the same as in case 1, $\mathbf{B}^e = \mathbf{B}^{0e}$), a null internal main field ($\mathbf{B}^m = \mathbf{0}$) and that the remaining contributions $\iota_n^m(\varphi)$ in eq. (10) contain only the Earth's magnetic field crustal contribution for SH degrees 15–65. In this example, the crustal field introduces an error that varies rapidly with longitudes but does not exceed 3 per cent (Fig. 1). The crustal field is therefore problematic for studying the field induced in the mantle if high frequencies are sought (Olsen 1999; Constable & Constable 2004; Kuvshinov *et al.* 2006).

The situation improves with the availability of more orbits because the longitude dependence of eqs (12) and (13) cancels out when the data are acquired on a spherical surface. For a rotating Earth, the LT is related to the difference in longitude between the subsolar point φ_s and the longitude φ of an observer (Hulot *et al.* 2007)

$$t = (180^\circ + \varphi - \varphi_s)/15. \tag{16}$$

The asymptotic limit of having an infinite number of data on a spherical surface is given when integrating the expression (12) over the subsolar longitudes

$$\widetilde{q}_w^0(t) = q_w^0(t) + \frac{1}{2\pi\,(2w+1)} \sum_{n=1}^{\infty} \sum_{m=0}^{n} \int_0^{2\pi} \iota_n^m(15t - 180 + \varphi_s) \left(\frac{a}{r}\right)^{n+w+1} \left\{(w+1)\beta_{w,n}^m - (n+1)\gamma_{w,n}^m\right\} \mathrm{d}\varphi_s. \tag{17}$$

Therefore, if the data sampling is good enough, we indeed converge towards the analytical estimation

$$\widetilde{q}_w^0(t) = q_w^0(t),$$

which is the true value at the LT t. For non-uniform data coverage in space and in time, which happens for drastic data selection criteria, the integral in the right-hand side of eq. (17) does not average out. This has some consequences on the separation of the internal and external fields (Olsen *et al.* 2010a). For recent Earth's satellite missions like CHAMP or Oersted, the complete coverage in space and in LT is achieved after about 130 and 790 days, respectively (Olsen *et al.* 2010b; Fig. 8). Not surprisingly the separation of the sources is not achievable when considering time windows too short to survey all longitudes (Schwarte *et al.* 2003, Fig. 3). Strictly speaking, internal and external magnetic field predictions in SH for shorter time scales may contain more or less artificial LT variations in the geocentric Earth fixed reference frame (representing the different contributions in the solar-magnetic and the geocentric-solar-magnetic reference frames may alleviate this issue; Maus & Lühr 2005 for a discussion).

4 IMPLICATIONS FOR CRUSTAL FIELD IDENTIFICATION

We now discuss how the error in estimating the large-scale internal and external fields described in the previous section impact on the identification of the crustal magnetic field signature. A crustal field reflects the magnetic properties of rocks lying in the crust. It is generally among the most difficult field to identify from space because it appears generally weak and dominated by small spatial scales whose geographical distribution can hardly be predicted in advance. In a sequential magnetic field analysis, the crustal contributions $\widetilde{\mathbf{B}}^c$ are mathematically defined as an anomaly with respect to the dominant magnetic fields that are represented by explicit models in SH. We have

$$\widetilde{\mathbf{B}}^c = \mathbf{B}(t) - (\widetilde{\mathbf{B}}^e(t) + \widetilde{\mathbf{B}}^m(t)). \tag{18}$$

Therefore, any uncorrected external or main field leaks into these residual measurements. In general, the main field is expressed in SH, the ionospheric field is discarded by selecting night time data only and the magnetospheric field with its induced internal part, present at day and night times, is estimated along some portion of the satellite half-orbit by numerical inversions (Maus *et al.* 2008) that is described here with eqs (6) and (7). In a sequential analysis, this ring current correction is essential because the domination of the magnetospheric field that varies rapidly in time renders impossible the identification of the anomaly field. Because the magnetic field measurements are in practice corrected for the magnetospheric field estimated along a portion of the satellite orbits, we will call this procedure hereafter the satellite along-track correction (so far we called it the along-track analysis). Replacing eqs (6) and (7) into (3), (4) and (5) gives the expression of the estimated symmetric external field that is used as a magnetospheric field correction

$$\widetilde{B}_r^{0e} = \sum_{n=1}^{\infty}\sum_{m=0}^{n}\sum_{w=1}^{2}\left\{\iota_n^m(\varphi)(n+1)\left(\frac{a}{r}\right)^{n+2} - n\varepsilon_n^m(\varphi)\left(\frac{r}{a}\right)^{n-1}\right\}\gamma_{w,n}^m P_w^0(\theta), \tag{19}$$

$$\widetilde{B}_\theta^{0e} = -\sum_{n=1}^{\infty}\sum_{m=0}^{n}\sum_{w=1}^{2}\left\{\iota_n^m(\varphi)\left(\frac{a}{r}\right)^{n+2} + \varepsilon_n^m(\varphi)\left(\frac{r}{a}\right)^{n-1}\right\}\beta_{w,n}^m\frac{\mathrm{d}P_w^0(\theta)}{\mathrm{d}\theta}, \tag{20}$$

$$\widetilde{B}_\varphi^{0e} = 0. \tag{21}$$

We see that the estimated ring current correction $\widetilde{\mathbf{B}}^{0e}$ is, again, explicitly contaminated by internal fields. In particular, it also depends on the true crustal field $\mathbf{B}^c$ as was already shown in Fig. (1). This is intuitively understood by noting that the crustal field, as any other magnetic field, theoretically averages out on a sphere (divergence free theorem) but not necessarily on a portion of the sphere; $\widetilde{\mathbf{B}}^{0e}$ thus contains a portion of all remaining internal contributions over all longitudes, including the crustal field. Therefore, the contamination by the crustal field will propagate to the estimated crustal field $\widetilde{\mathbf{B}}^c$ after correction for the estimated external field (eq. 18).

4.1 Data gridding and anomaly maps

There are many cases in planetary magnetism where the magnetic data corrected along the satellite tracks are not modelled but mapped at a mean altitude (Langel & Hinze 1998; chap. 6). Depending on the care taken to remove all other fields, the problems raised by the along-track filtering are more or less prominent. We discuss this difficulty in more qualitative and quantitative details for the Lunar, Mars and Earth's crustal fields.

The mapping of the Moon's crustal magnetic field is difficult because the physics of the total magnetic field is poorly understood in details and the number of available data are not sufficient to make an objective and extensive parametrization of the magnetic sources. In particular, the solar wind and the near Earth's magnetic environment hide the crustal signal that is too small and weak to be represented in SH directly from the data without correcting them for the external field (Purucker & Nicholas 2010). We selected Lunar prospector data (Binder 1998) only in the wake and tail regimes and corrected the data for a zonal external field estimated up to SH degree $w = 2$ by least squares along the Lunar Prospector tracks (this real case approximates the formal asymptotic expression given by eq. 19 for the radial component). In Fig. (2), we see that the correction allows us to unveil partly some details that are likely to be of crustal origin. We note however that the overall result remains noisy and that it displays north-south trends parallel to the track lines that are probably because of complex large-scale

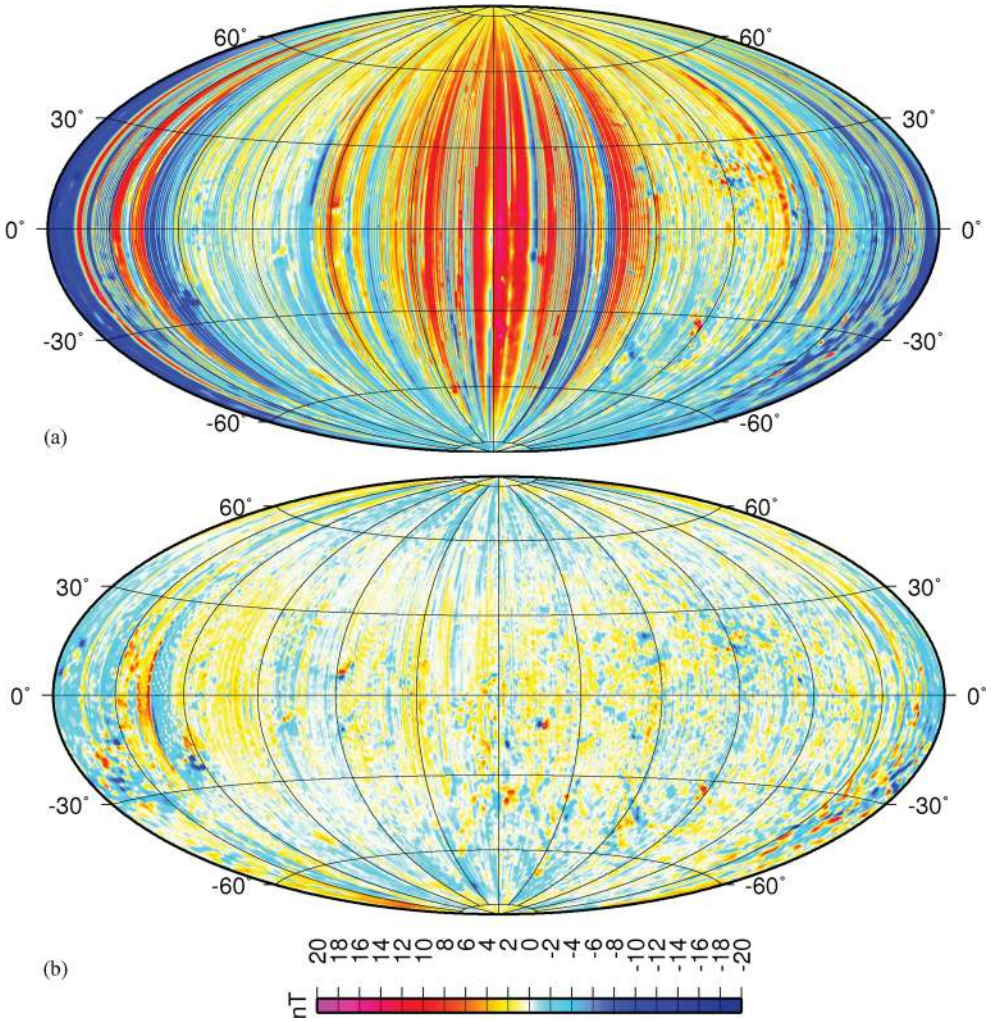

Figure 2. (a) Raw Lunar Prospector vector data (radial component) between 1999 January 1 and 1999 July 29. (b) Radial component of the anomaly field after data selection in the wake and the geomagnetic tail, and a correction for a global internal and and external field (to SH degree 2) track-by-track. Projection is Hammer–Aittof.

magnetic fields that could not be modelled by our subset of functions. We conclude for now that field external to the Moon is so dominant over the crustal field ($|\mathbf{B}^e| \gg |\mathbf{B}^c|$) that the along-track correction, although imperfect, brings some improvements.

The situation for Mars is the opposite one as the planet has a dominant crustal field (Langlais *et al.* 2004) and, in general, weak external fields (Acuña *et al.* 1999). The geometry of the Mars' external field is not well understood but the along-track procedure is sometimes applied to clean the data (Hood & Zakharian 2001; Connerney *et al.* 2005; Lillis *et al.* 2010). In Fig. (3), we map the Mars' magnetic field as it is measured by Mars Global Surveyor (MGS; Acuña *et al.* 1999) between altitudes 348 and 422 km and years 1999 and 2003 during the MO phase and night times. The bottom picture shows the radial component, $\widetilde{B}_r^{0e}$, of the external field estimated along each MGS track by least squares to SH degree $w = 2$ (This real case is, as above, a numerical approximation of the formal inverse problem described by eq. 19 for the radial component). Clearly, the estimated external field is correlated with (therefore contaminated by) the largest Mars' crustal field signatures. The radial dependence of the along-track analysis is less prominent but appears as a spatial variation correlated with the MGS altitude, lower in the Southern than in the Northern hemisphere. The estimated external field is therefore mostly artificial and the benefit of this external field correction is doubtful. The message conveyed here is that the along-track procedure does not only remove genuine large field signatures as it is generally thought (Purucker & Dyment 2000) but adds an anisotropic noise to the data. These pseudo magnetic anomalies are characterized by offsets appearing between adjacent satellite passes that may be easily enhanced when computing horizontal derivatives or downward continuation of the field to the surface and then wrongly interpreted in terms of crustal magnetic field discontinuities. In this case, the spectral leakage is large because the crustal field dominates the total magnetic field signal ($|\mathbf{B}^e| \ll |\mathbf{B}^c|$).

The Earth represents an intermediate case between the Moon and Mars. Because $|\mathbf{B}^e| \geq |\mathbf{B}^c|$, the benefits of a first-order external field correction along the half-orbit is certain but this correction, as in the case of Mars, is correlated with the crustal field (Thébault *et al.* 2010). To better quantify the artefacts and keep track on their shapes throughout the following discussion, we return to the idealized cases described by the analytical eqs (19) and (20). We consider for now that both the main and external fields are zero along all meridians. We investigate how the estimated crustal field contaminates itself along a pole-to-pole analysis. The 'true' Gauss coefficients are given by the CM4 crustal model

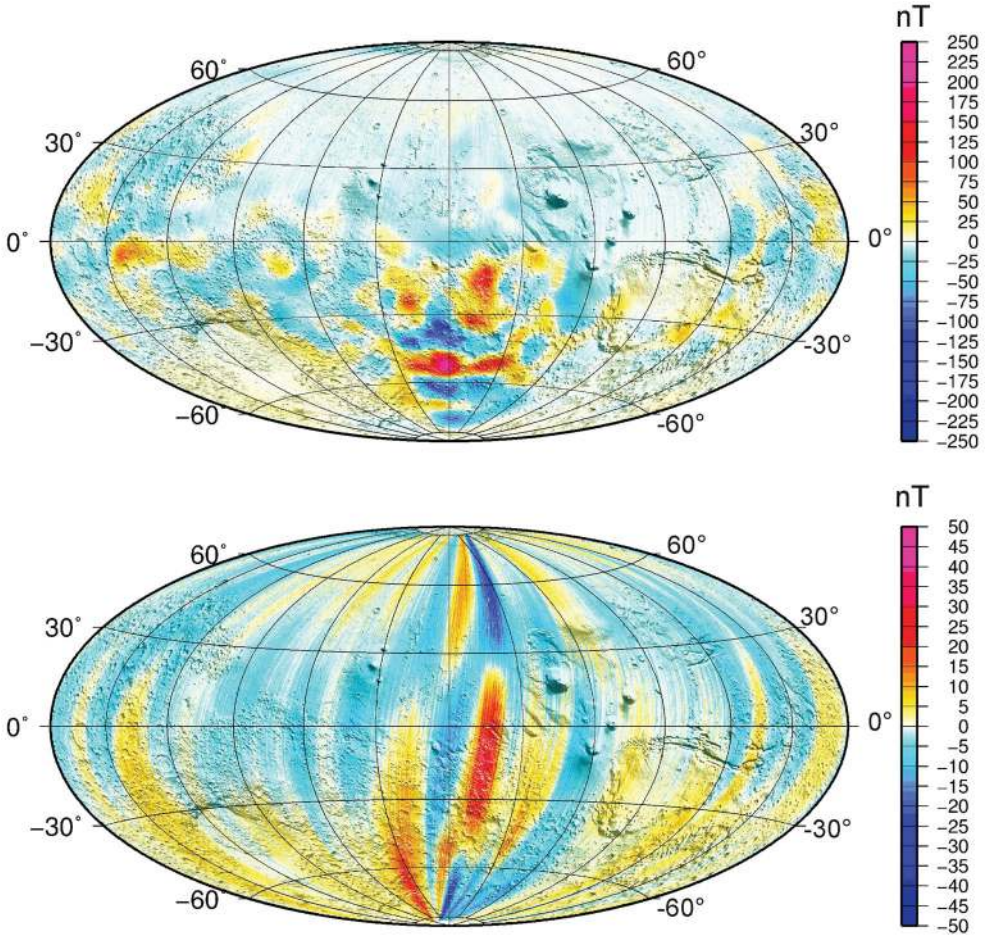

Figure 3. Top panel: map of the radial component of the magnetic field of Mars observed by MGS satellite between 350 and 430-km altitude. Bottom panel: the radial external field correction $\widetilde{B}_r^e$ estimated along the satellite pole-to-pole path. Projection is Hammer–Aittof.

for SH degrees 15–65. We proceed as if we did not know that external contributions were zero and we estimate a symmetric external field with eqs (19) and (20) up to $w = 2$. Fig. (4) compares the CM4 vertical crustal component before and after correction at 400 km altitude. The two maps are globally consistent but the 'corrected' one is overall more fuzzy and some anomalies, like in the Atlantic Ocean, are significantly skewed. The bottom figure displays the regions where the external field correction introduced a change of sign in the radial component. The magnetic anomalies over oceans, particularly over the Pacific, are more damaged because they are weaker than over continental areas. This has important practical implication as magnetic measurements remain one of the few means to access the bulk properties of the oceanic crust. The weak anomalies have a special interest because they have spatial scales comparable with those detected by marine or aeromagnetic measurements. So far, however, it has not been possible to reconcile satellite and near-surface magnetic crustal field observations (Hamoudi *et al.* 2007; Fig. 4 and Maus *et al.* 2007a; Fig. 7). Part of the general incompatibility between near surface and satellite data at regional scales could be because of the satellite along-track correction (or, equivalently, to the aeromagnetic correction along the flight lines) although it is clear that a significant error also comes from complex fields detected differently at satellite, airplane or ship altitudes. Fig. 5 (left-hand panel) displays the vertical component of the difference between the corrected and uncorrected crustal fields (this is therefore the external field estimated along the half-orbits described by eq. 19). Applying an along-track correction to data containing only crustal contributions creates an artefact reaching 4 nT at 400 km altitude. This value is low compared to the total Earth's magnetic field but is several orders of magnitude larger than the accuracy of satellite magnetometers and comparable to the Earth's crustal field that reaches about 20 nT at this altitude. This analysis shows that it is important in practice to remove a first-order crustal field model before performing a satellite along-track correction for the external field to lower the level of spectral leakage. However, this solution is not fully effective when the remaining crustal field residuals do not average out along each orbit, unless the average is lower than the data accuracy. In practice, the data selection being performed according to magnetic proxies quantifying the magnetic activity (for instance, Thébault 2006), it may happen that data are selected only along small portions of a half-orbit. These data should be discarded because the remaining crustal field has little chance to cancel out over small segments of the satellite half-orbit.

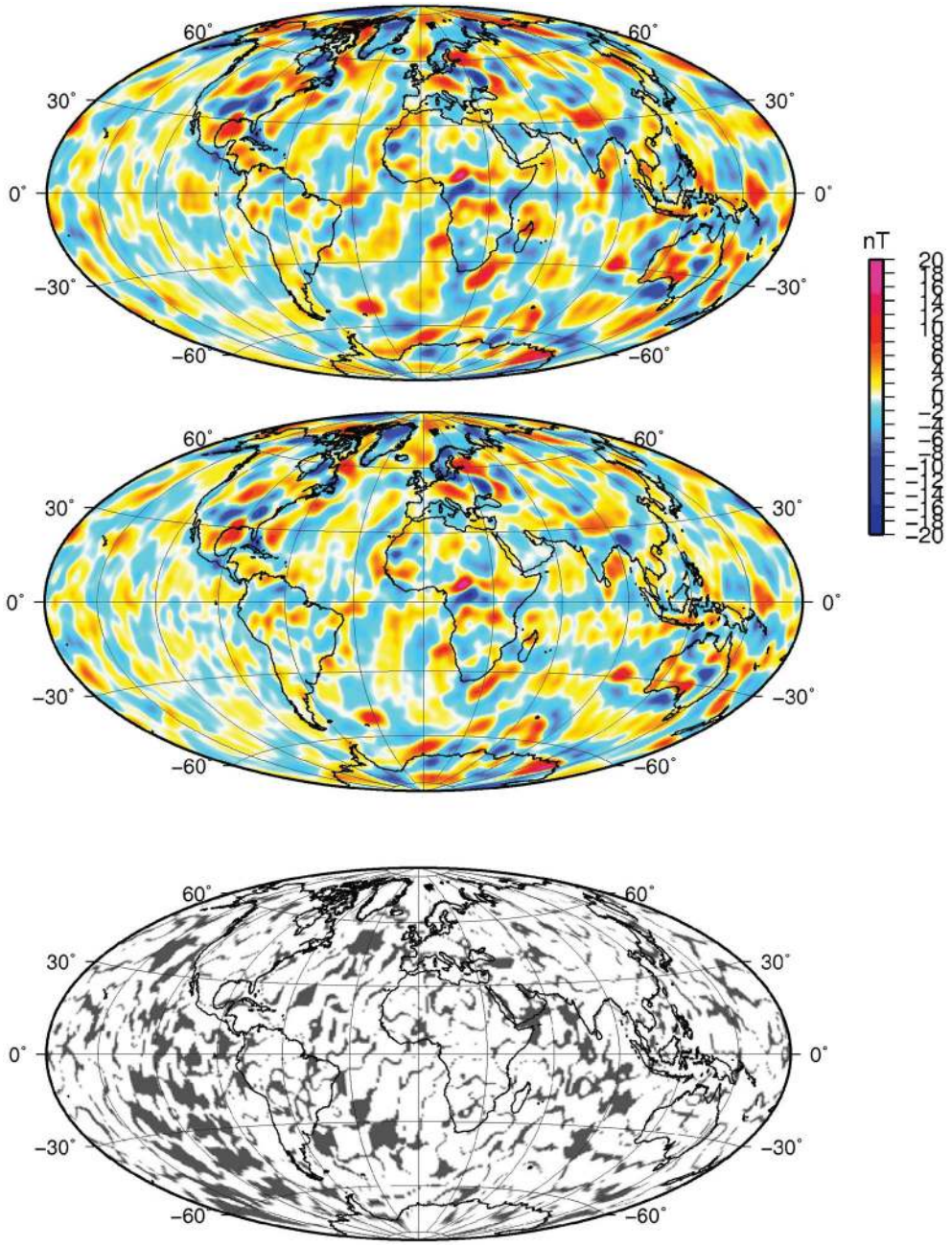

Figure 4. Radial component of the CM4 crustal field model (Sabaka *et al.* 2004) for SH degree 15–65 before (top panel) and after the filtering along a complete half-orbit (middle panel; see text for details) . The bottom panel highlights the regions where the sign of the magnetic field was changed by the filtering process. Projections are Hammer-Aittof.

4.2 SH models of the anomaly field

Modelling the data with a global potential field method, be it in SH, fortunately allows us to partly remove the fictitious signals added to the data by the along-track correction for a global internal and/or external field. A calculation (by substituting eqs 6 and 7 into 1) indeed would show that the estimated correction field does not solve the Laplace equation, despite the care taken to choose an expression of $\mathbf{B}^e$ based on a physical justification (a zonal field expanded in SH). Fig. (5) compares the vertical component of the external field correction $\widetilde{\mathbf{B}}^{0e}$ obtained analytically (see previous paragraph) with the residuals between a SH crustal field model and a set of real CHAMP satellite vector data that underwent a correction for the main field and an along-track correction for the magnetospheric field (Thébault 2006). The two pictures have similarities although they are not readily comparable because the external field correction is applied in the real case on noisy measurements, includes higher SH degrees and orders, and is performed in an inclined reference frame along true satellite (incomplete) half-orbits. This comparison nevertheless provides some confidence that the fictitious features are not totally expressible in SH because they are found in the residuals between the crustal field model and the data. Because we cannot exclude that part of the error contaminate the crustal field model

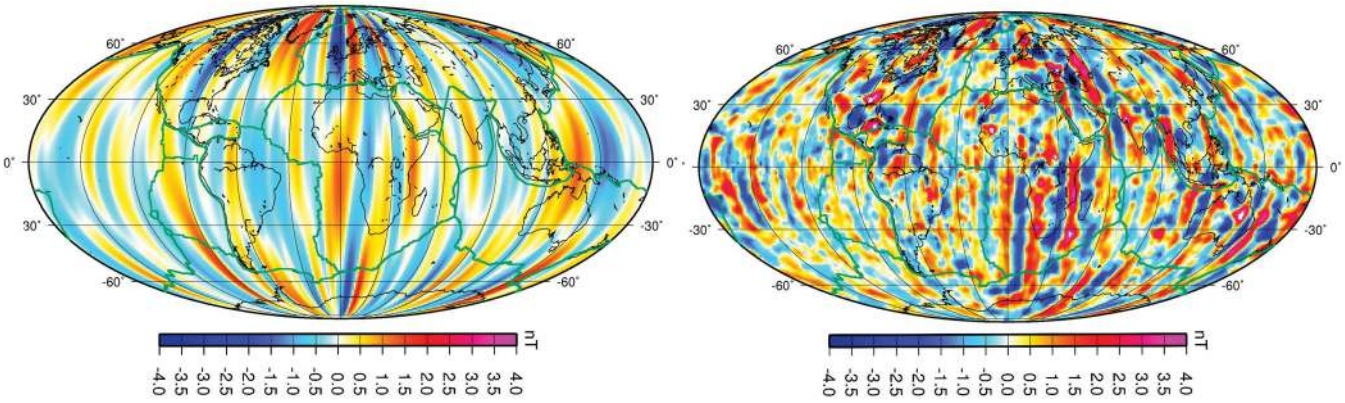

Figure 5. Left-hand panel: estimate of the artefacts created by the track-by-track correction for the external field and its induced part. This is calculated at 400 km altitude from equation (19) on the Z component ($-B_r$) with a set of lithospheric field coefficients using the CM4 comprehensive crustal field model (Sabaka *et al.* 2004) for SH degree 15–65. Right-hand panel: distribution of residuals on the Z component after inversion of a set of track-by-track corrected CHAMP satellite data (see Thébault 2006). Projection is Mollweide.

even after a SH modelling, we quantify the shape and the strength of these remaining artefacts that we define by $\mathbf{B}^a$. Part of these artefacts may be expanded in SH and can be expressed as the gradient of a potential

$$V^a = a\sum_{l=1}^{\infty}\sum_{k=0}^{l}\left(\frac{a}{r}\right)^{l+1}\left\{\rho_l^k\cos(k\varphi)+\sigma_l^k\sin(k\varphi)\right\}P_l^k(\theta). \tag{22}$$

The Gauss coefficients ρ_l^k and σ_l^k of V^a minimize $\chi^2 = \|(\widetilde{\mathbf{B}}^c - \mathbf{B}^c) - \mathbf{B}^a\|^2_{\partial\Omega}$ over a spherical surface $\partial\Omega = \{0 \le \theta \le \pi, 0 \le \varphi \le 2\pi, r = \text{Constant}\}$. We recall that $\mathbf{B}^c$ is the true crustal field and $\widetilde{\mathbf{B}}^c$ its estimation in SH after imperfect data correction for the other source fields (eq. 18). $\widetilde{\mathbf{B}}^c$ therefore contains the artefacts introduced by the correction. We consider for more generality that main and external field correction errors may also subsist. Solving formally this inverse problem on the surface of a sphere, we show that

$$\begin{aligned}\begin{Bmatrix}\rho_l^k\\ \sigma_l^k\end{Bmatrix} = &\sum_{w=1}^{2}\sum_{n=1}^{\infty}\begin{Bmatrix}g_n^k\\ h_n^k\end{Bmatrix}\left(\frac{a}{r}\right)^{n-l}\left\{\frac{(l+1)(n+1)\gamma_{w,l}^k\gamma_{w,n}^k\left\|P_w^0\right\|^2+\beta_{w,l}^k\beta_{w,n}^k\left\|\mathrm{d}P_w^0/\mathrm{d}\theta\right\|^2}{(2l+1)(l+1)\left\|P_l^k\right\|^2}\right\}\\ &+\sum_{w=1}^{2}\sum_{n=1}^{\infty}\begin{Bmatrix}q_n^k\\ s_n^k\end{Bmatrix}\left(\frac{r}{a}\right)^{n+l+1}\left\{\frac{-n(l+1)\gamma_{w,l}^k\gamma_{w,n}^k\left\|P_w^0\right\|^2+\beta_{w,l}^k\beta_{w,n}^k\left\|\mathrm{d}P_w^0/\mathrm{d}\theta\right\|^2}{(2l+1)(l+1)\left\|P_l^k\right\|^2}\right\},\end{aligned} \tag{23}$$

with $\gamma_{w,l}^k$ and $\beta_{w,l}^k$ defined by eqs (8) and (9).

Several conclusions may be drawn from the idealized solution given by eq. (23). First, part of the artefacts caused by errors in correcting for internal and external fields, indeed leak into internal SH models because the coefficients $\{\rho_l^k, \sigma_l^k\}$ are analytically different from zero. The contamination affects all harmonics, a characteristic of spectral leakage, and we confirm that its strength depends on the satellite altitude. Secondly, the magnetic field component B_φ^c, which did not bear the along-track correction, is finally altered when the corrected data are represented in SH. This may be an important side effect because this component, perpendicular to the satellite synthetic orbits, constrains the sectorial contributions $n = m$. At last, we see that, if the coefficients g_n^m and h_n^m describe the 'true' crustal field, their estimations $\widetilde{g}_l^m$ and $\widetilde{h}_l^m$ after along-track correction are

$$\begin{Bmatrix}\widetilde{g}_l^m\\ \widetilde{h}_l^m\end{Bmatrix} = \begin{Bmatrix}g_l^m\\ h_l^m\end{Bmatrix} - \begin{Bmatrix}\rho_l^m\\ \sigma_l^m\end{Bmatrix}. \tag{24}$$

Therefore, depending on the sign of $\{\rho_l^k, \sigma_l^k\}$, the crustal field could be over- or underestimated. Replacing eq. (23) into (24) and assuming for a while that $q_n^m = s_n^m = 0$ (no external field contamination), we obtain

$$\begin{Bmatrix}\widetilde{g}_l^m\\ \widetilde{h}_l^m\end{Bmatrix} = \begin{Bmatrix}g_l^m\\ h_l^m\end{Bmatrix} - \sum_{w=1}^{2}\sum_{n=1}^{\infty}\begin{Bmatrix}g_n^m\\ h_n^m\end{Bmatrix}\left(\frac{a}{r}\right)^{n-l}\left\{\frac{(l+1)(n+1)\gamma_{w,l}^m\gamma_{w,n}^m\left\|P_i^0\right\|^2+\beta_{w,l}^m\beta_{w,n}^m\left\|\mathrm{d}P_w^0/\mathrm{d}\theta\right\|^2}{(2l+1)(l+1)\left\|P_l^m\right\|^2}\right\}, \tag{25}$$

showing the contamination of the crustal field by itself caused by the along-track correction. Note that eq. (25) is an illustration of a conclusion given by Sabaka & Olsen (2006; Fig. 1) who state that the SH models obtained from serial analyses tend to have power spectra different from those obtained in a more comprehensive way.

4.3 Comparisons between initial and the estimated anomaly fields

To determine if the crustal field is globally over- or underestimated, we compare the initial and the corrected crustal fields in the spectral domain using three criteria described by Sabaka & Olsen (2006): the spatial magnetic field power spectrum (which measures the energy carried out by each degree n), the SH correlation (which measures degree by degree the correlation between two models) and the sensitivity

matrix (that displays the difference in per cent of Gauss coefficients for each degree and order). We compute the SH coefficients $\{\rho_l^m, \sigma_l^m\}$ of the artefacts with eq. (23) by simulating different realistic sets of values $\{g_n^m, h_n^m\}$ and $\{q_n^m, s_n^m\}$ for the main and external fields and then we calculate the values of the internal coefficients $\{\widetilde{g}_l^m, \widetilde{h}_l^m\}$ after each correction of a zonal field along the satellite half-orbit with eq. (24). The analytical along-track filter (eq. 25) is applied at radius $r = a + 400$ km.

First, we consider only the CM4 crustal field for SH degree 15–65 and assume that all main internal and external coefficients are zero. Compared to a real data situation, this means that the data are perfectly corrected for the main and the external fields. In the second case, we add the difference between two main field models given by GRIMM2 (Lesur *et al.* 2010) for epoch 2005.5 and 2006, for degrees 1–14 as above, with external coefficients set to zero. This represents a case for which an error was made in correcting the measurements for 6 months of main field secular variation. In the third case, the main field coefficients from 1 to 14 are set to zero (not the crustal ones) and the external field coefficients are obtained from the CM4 magnetospheric field model at epoch 2001.0 with $Dst = -30$ nT up to SH degree 10.

We highlight these three particular cases but also explore other possibilities: a number of 2000 different combinations of coefficient values are evaluated with each of the main and external coefficients drawn from the normal distributions $\mathcal{N}(0, g_n^m)$ and $\mathcal{N}(0, q_n^m)$, where the g_n^m, q_n^m (respectively for h_n^m and s_n^m) are the coefficients of the second and third cases; the crustal field coefficients are always left unchanged. These random cases aim at showing the effect of a large variety of imperfect main and external field data corrections that could contaminate the final estimation of the crustal field after satellite along-track correction.

Fig. 6 (top panel) shows the power spectra at the Earth's surface of all input simulations. The bottom panel shows the power spectra of the estimated internal crustal magnetic field $\{\widetilde{g}_l^m, \widetilde{h}_l^m\}$ after the analytical correction along the half-orbits computed with eqs (23) and (24). The first case, involving perfect main and external field corrections, shows that the along-track correction introduces spurious SH degrees between 1 and 15. These artefacts are caused by a spectral leakage of the crustal field SH into the low degrees. The power spectrum after along-track analysis is underestimated but the cumulated difference at the Earth's surface (∼6 nT), is low compared to the root mean square (∼43 nT) of the initial crustal field. The first and third cases differ significantly only between SH degrees 15 and 30. However, the second case and the results of the 2000 random samples indicate that internal field contributions at low SH degree in the initial 'data' more often lead to the overestimation of the crustal field power spectrum after along-track filtering. Interestingly, the processing of real satellite measurements, which necessarily involves imperfect corrections for the internal and external fields, shows that crustal field power spectra derived in a sequential way have systematically less power than those derived comprehensively (Hemant & Maus 2003); a property predicted formally by Sabaka & Olsen (2006). Our numerical results suggest (at least when the correction is restricted to zonal terms and degree 2 as was done here) that the along-track correction may also reduce the power spectrum of the estimated crustal field but only marginally and under certain circumstances only. Comparisons between crustal models estimated using a comprehensive and a sequential approach from simulated satellite orbits and data in the framework of the Swarm preparation study (Friis-Christensen *et al.* 2006) also showed less differences than in real cases (Maus *et al.* 2002; Fig. 1; see also Sabaka & Olsen 2006; Fig. 3). We are bound to conclude that part of the difference observed between the crustal magnetic field power spectra has to be explained by the difference in the data selection and the regularization of the inverse problem rather than in the sole application of the along-track correction. In addition, eq. (23) also applies to a class of comprehensive inversions. When the internal or external field time parameterization reaches the limit of the data resolution (when only one or few orbits are available within the smallest time interval parametrized by the comprehensive model) a comprehensive inversion behaves similarly to an along-track analysis because the parameters are constrained by very few orbits. Therefore, we cannot rule out that some crustal models obtained in a comprehensive way may produce overestimated power spectra. Interestingly, Fig. 6 (bottom) shows that zigzag power spectra are symptomatic of spectral leakage—this zigzag features results from the orthogonality properties of the associated Legendre functions in $\gamma_{w,n}^m$ and $\beta_{w,n}^m$ (eqs 8 and 9) that depend on the parity of (w, n, m)—this provides a useful diagnosis tool for visually assessing the robustness of crustal field models obtained in a sequential or in a comprehensive way.

We finally focus on a case that produces an underestimated crustal field power spectrum (first case considering that data contain crustal field only). The SH correlation coefficient, which evaluates the agreement in direction between the initial and the corrected sets of Gauss coefficients, does not indicate systematic errors along the SH degrees (Fig. 7, top panel). However, the sensitivity matrix teaches us that the errors are distributed along SH degrees of equal orders m (Fig. 7, bottom panel). In the spatial domain, this corresponds to sectors of longitudes (Fig. 8). Apart from the Polar Regions, where the largest errors occur, the mid-latitude linear stripes are in excess of 5–10 nT in the oceanic regions at the Earth's surface. These numbers derived from eq. (24) are, again, slightly underestimated compared to an analysis along real orbits. The reader is referred to Maus *et al.* (2006) for more realistic figures obtained in a synthetic case with incomplete real orbits, and to Lesur *et al.* (2008; Fig. 9) for a real data analysis. Both works display the same features as in Fig. 8 with strength reaching twice as much as our rough prediction. The spatial scales of these stripes is problematic if we believe that some of the largest magnetic lineaments in oceanic regions are detected by low Earth orbiting satellites. The artefacts may be visually distracting when they coincidentally align with oceanic ridges, in the South Atlantic ocean, for instance. This may also have consequences for by-products, like maps of magnetization or magnetic crustal thickness. The World Digital Magnetic Anomaly map (WDMAM; Korhonen *et al.* 2007), for example, is an international effort made towards compiling and merging the magnetic information measured from marine, airborne and satellite platforms (Hamoudi *et al.* 2007; Hemant *et al.* 2007; Maus *et al.* 2007, 2009). By construction, wavelengths exceeding about 400 km in the WDMAM map are supplied by satellite-based crustal models. In this context, it seems important to sort out between the genuine magnetic field structures and the inherent limits of the satellite along-track correction. It is noteworthy that the SH least-squares solution properly restored the sign of the magnetic anomalies that was occasionally inverted by the along-track correction (compare Figs 4 and 8). This assertion must certainly

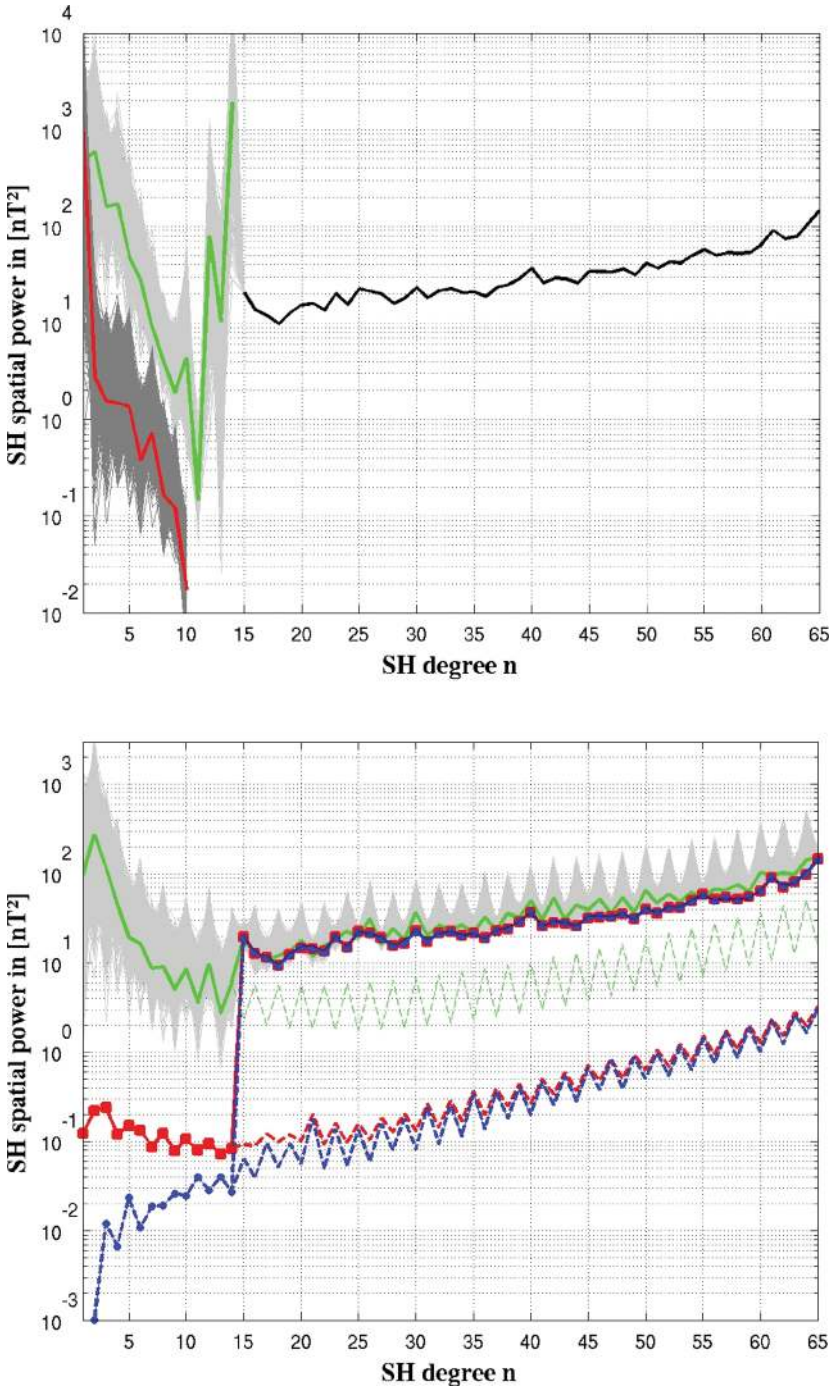

Figure 6. Top panel: Power spectra of the CM4 crustal field model (Sabaka *et al.* 2004) for SH degree 15–65 (in black), of the difference between the GRIMM2 model (Lesur *et al.* 2010) between epochs 2005.5 and 2006 for SH degree 1–14 (in green) and the CM4 magnetospheric field to SH degree 10 at epoch 2001.0 (in red). The light and dark grey curves are the spectra of 2000 internal and external field correction errors computed randomly (see text for details). Bottom panel: the power spectra of the estimated internal anomaly field after along-track correction in cases 1 (blue circles), 2 (green) and 3 (read squares) that are discussed in the text. The power spectra of the difference between the CM4 crustal field model and the estimated anomaly field models after along-track filtering for the three cases is shown by the dashed curves. The grey curves are the power spectra of the 2000 anomaly fields that are computed after along-track filtering using the 2000 different main and external field contaminations shown in the top figure.

be tempered in a real data situation involving partial orbits only, scalar anomaly data and above all when the magnetic field measurements corrected along the orbits are modelled at regional or continental scales using dedicated methods (Schott & Thébault 2010, for a review). In this respect, Figs 4 and 5 show for the Earth the general distribution of the error introduced by the ring current correction along the satellite tracks.

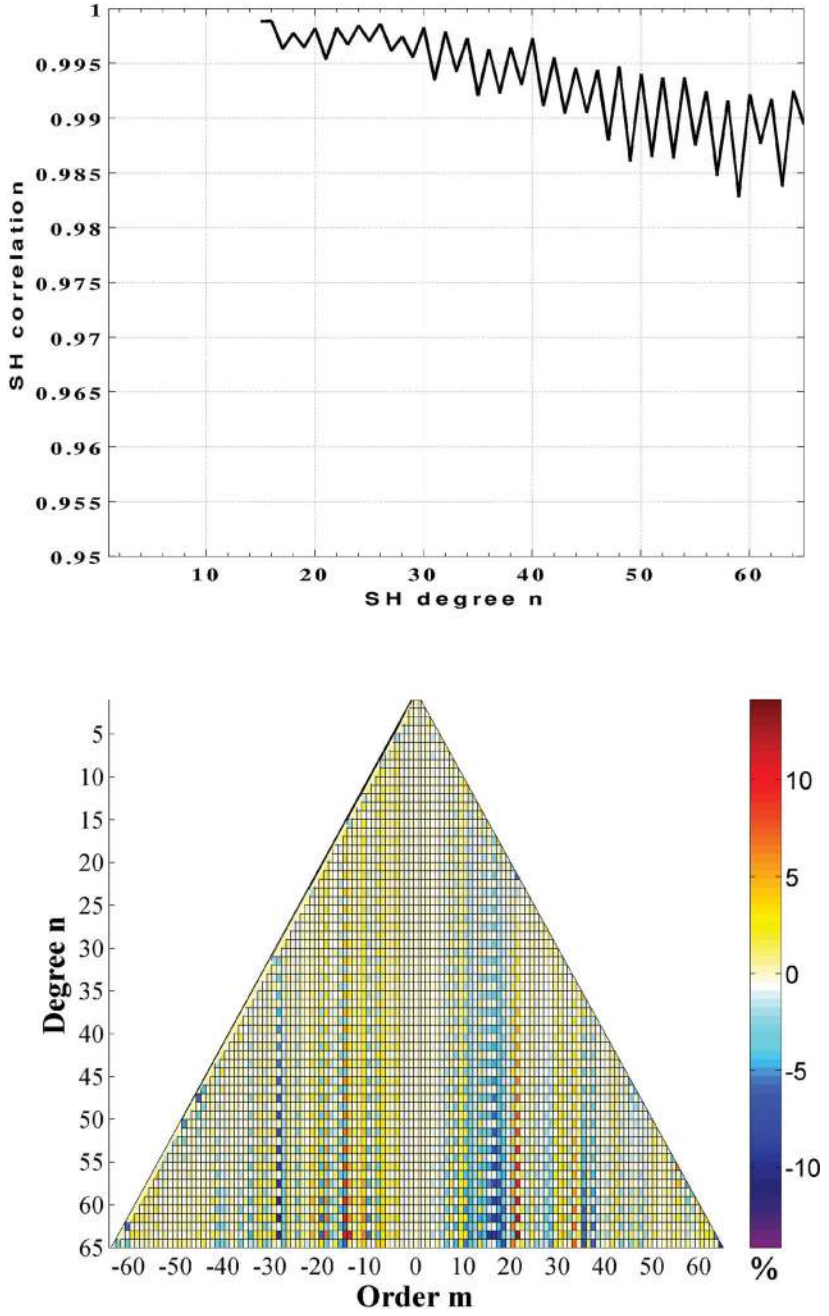

Figure 7. Top panel: spherical harmonic correlation analysis between the initial CM4 (black curve in Fig. 6 – top panel) and the estimated crustal field models after along-track correction for the first case (blue curve in Fig. 6 – bottom panel). Bottom panel: sensitivity matrix showing the error in per cent between the initial CM4 crustal field model and the estimated anomaly field for case 1.

5 DISCUSSION

In this paper, we have reviewed some of the issues raised by the spectral leakage caused by analysing magnetic field measurements along a satellite half-orbit. The spectral leakage arises because estimating a model via a truncated series expansion is, in general, an ill-posed problem. In this respect, our conclusions drawn for geomagnetism apply to any signal studied over a finite portion of the sphere and the formulae, with slight convention changes, would also apply to any physical quantity developed in SH (topography, gravity field, seismic tomography, etc.). In the framework of planetary magnetism, we confirmed that the along-track analysis applied on data over a full or a portion of a satellite half-orbit reduces the magnetic field power of the static magnetic field at all SH degrees and orders. However, this loss of power is, in general, rather low and occurs less often than an overestimation of the power spectrum that prevails when there is a strong contamination of other source fields. More importantly, this analysis introduces fictitious wavelengths because of the redistribution of the energy of some harmonics among others. In general, this creates spatial distortions in the final magnetic field model that, when considering the static and weak Earth's lithospheric magnetic field for instance, may lead to erroneous geophysical interpretations. Fortunately, the shape of the artefacts can be

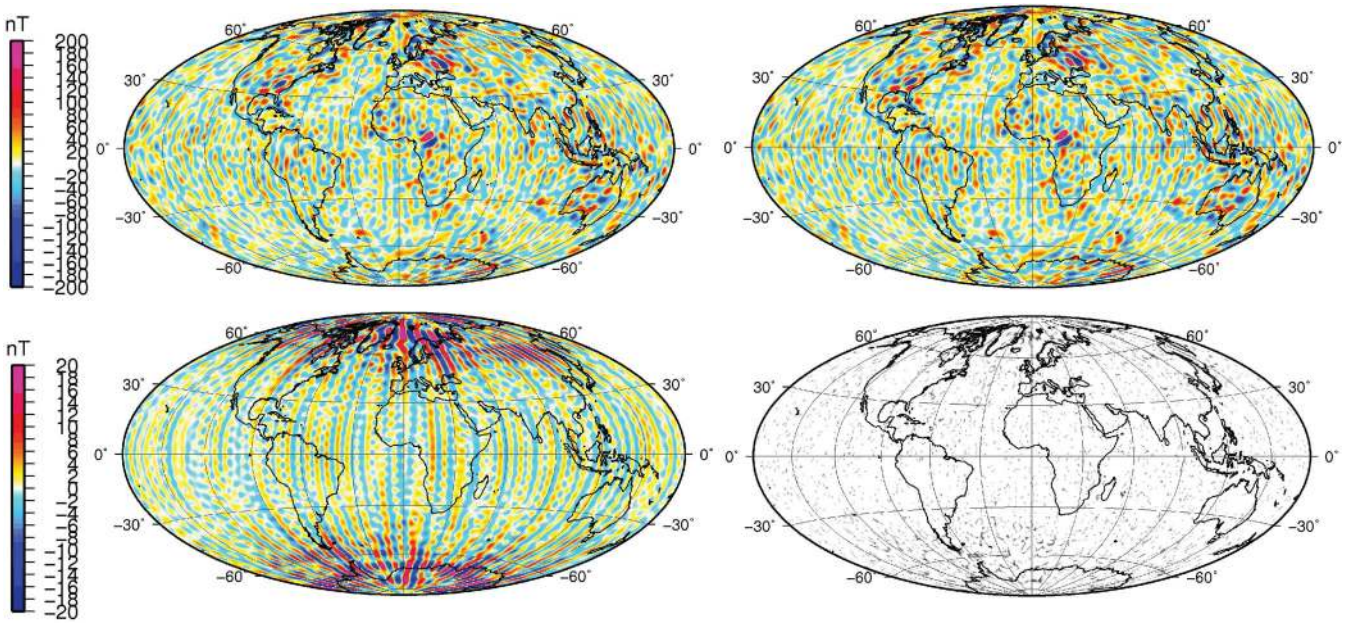

Figure 8. Top left-hand panel: radial component of the CM4 model at the Earth's mean radius. Top right-hand panel: the along-track filtered CM4 computed with eqs (23) and (24). Bottom left-hand panel: difference between the initial and the filtered CM4 model. Bottom right-hand panel: regions where a change of sign persists after the SH modelling on a sphere. All pictures are sketched at the Earth's mean radius in a Hammer–Aittof projection.

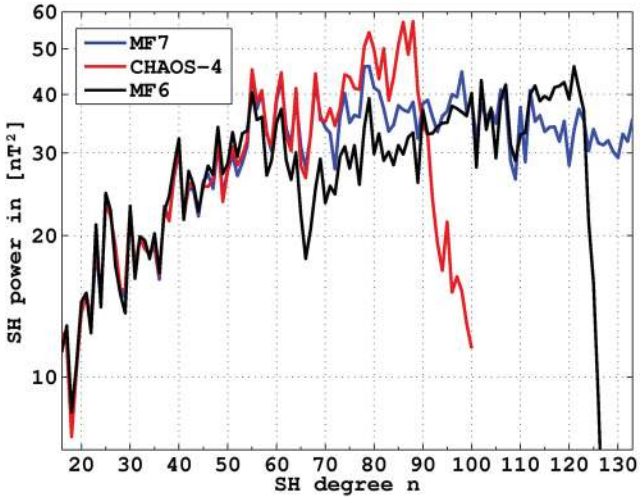

Figure 9. Power spectra of two yet unpublished recent lithospheric field models CHAOS-4 (N. Olsen, personal communication, 2011) and MF7 (S. Maus, personal communication, 2011). Both models are now in close agreement up to SH degree 70 contrary to the MF6 model (Maus *et al.* 2008) that shows a loss of power around degree 60 (see the text for a discussion).

identified and is often similar to Fig. 5 for polar orbiting satellites. The artefacts are however more pernicious when considering the spatial and the time variation of the magnetic field as spatial variation may appear as time variations and conversely.

The setting of an along-track analysis is simple but a careful protocol must be followed to mitigate the artefacts. First, it is crucial to lower the errors by correcting the measurements for all unwanted magnetic fields before trying to identify a subset of SH harmonics by an along-track analysis. The along-track analysis should not be used as a low pass or bandpass filter because it fails in extracting accurately one specific set of harmonics. This implies that all corrections should be performed using, if possible, explicit models that were co-estimated with the same data set. From a theoretical viewpoint, this means that the comprehensive inversion method is in principle superior to any other method. Therefore, empirical methods such as the along-track correction should only try to improve the local resolution of the magnetic field models, when the signal-to-noise ratio becomes globally too small (or, of course, when no alternative exists but then one may easily question the choice of the selected parameters and the relevance of the model obtained). Second, the coefficients estimated along the orbits do not theoretically covary for the SH orders $m = 0$ (i.e. the SH are orthogonal along a single meridian). We should therefore restrict the along-track analysis to these harmonics (note that this general rule is true for polar orbits only). This also implies that only large portions of a satellite half-orbit should be analysed to ensure that the separation of the harmonics is numerically achievable. If the analysis is done on small portions of the half-orbit or to higher SH orders m, the covariance between the harmonics will amplify the magnitude of the error and make

the geographical distribution of the artefacts more complex. Given these considerations, we warn against the application of the along-track filtering technique on scalar measurements because the SH magnetic field contributions are theoretically not separable using this component even for the order $m = 0$ and for a full half-orbit.

These considerations certainly restrict the scope of the along-track analysis. However, despite these shortcomings, the along-track analysis may be a rewarding technique when applied carefully. The sequential MF6 model, for example, is based on a stringent data selection and is expanded to SH 120 (Maus *et al.* 2008) whereas published comprehensive models are derived to about SH degree 65 (and agree to say, SH degree 50; Thébault *et al.* 2010). This does not mean that all harmonics of the MF6 model are well resolved—some of them being strongly regularized from SH degree 80—but this tentative model shows encouragingly some regional correlations between magnetic anomalies and small-scale continental geological bodies (Maus *et al.* 2008). Yet, the MF6 model exhibits a sudden loss of power from SH degree 60 (Fig. 9) that can be interpreted as a consequence of the along-track correction for the magnetospheric field embedded in the processing. This feature is in fact because of data selection. The outlier CHAMP data used to build the MF6 model were identified against the MF5 model (Maus *et al.* 2007b) that was itself obtained (Maus *et al.* 2007b, Section 2.7) using an outlier detection against the MF4x model (Lesur & Maus 2006). However, the MF4x is expanded to SH 60 in the polar regions and to SH degree 90 in the equatorial regions to account for the geographical distribution of the signal noise. This is the major reason why the power spectrum is low in this waveband. This demonstrates again if necessary that the data selection plays the most prominent role in magnetic field modelling. The more recent MF7 model (yet unpublished) is expanded to SH degree 133 and compares well with the recent comprehensive-like CHAOS-4 model (Olsen *et al.* 2010, AGU) to SH degree 70 (Fig. 9). There is at present no better reason to suspect an underestimation of the MF7 power spectrum rather than an overestimation of the CHAOS-4 model. The CHAMP data used to derive the MF7 lithospheric field model were processed using a satellite along-track correction after the co-estimation of a main field model, an external field model, and a lithospheric field model to SH degree 80 (S. Maus, personal communication, 2011). The along-track correction iterates over a co-estimation of all known source fields. This flow of processing follows the sequence that is suggested by our study.

The theoretical problem of spectral leakage along the satellite tracks will always be present, but may be considerably alleviated by multi-point observations according to eq. (12) and (13). In a recent paper, Thomson *et al.* (2010) obtained a lithospheric field model with apparently reduced east-west artefacts making use of magnetic observatory data available worldwide in their data correction for the external field (their model, however, exhibits an unexpected low-power spectrum between SH degree 30 and 40, see their Fig. 6). The forthcoming Swarm satellite constellation will further improve the situation for the Earth by delivering three simultaneous measurements along different polar orbits (Friis-Christensen *et al.* 2006). All simulations performed so far during the scientific preparation of this mission demonstrate that its configuration will considerably enhance the reliability of magnetic field models by allowing a better separation of the source field components and reducing the problem of spectral leakage (Olsen *et al.* 2006).

ACKNOWLEDGMENTS

This work was partly funded by CNES. We would like to thank P. Alken, B. Langlais, T. Sabaka and M. Evrett for providing constructive comments and A. Fournier for an early review of this manuscript. For IPGP this is contribution number 3238.

REFERENCES

Acuña, M.H. *et al.*, 1999. Global distribution of crustal magnetism discovered by the Mars Global Surveyor MAG/ER Experiment, *Science,* **284,** 790–793.

Arkani-Hamed, J., Langel, R.A. & Purucker, M.E., 1994. Scalar magnetic anomaly maps of Earth derived from POGO and Magsat data, *J. geophys. Res.,* **99**(B12), 24 075–24 090

Ashour, A.A., 1964. On some formulae for integrals of associated Legendre functions, *Q. J. Mech. appl. Math.,* **17**(4), 513–523, doi:10.1093/qjmam/17.4.513.

Balasis, G., Egbert, G.D. & Maus, S., 2004. Local time effects in satellite estimates of electromagnetic induction transfer functions, *Geophys. Res. Lett.,* **31,** L16610, doi:10.1029/2004GL020147.

Binder A.B., 1998. Lunar Prospector: overview, *Science,* **281,** 1475–1476.

Cain, J.C., 2007. P-OGO (OGO-2, -4 and -6 spacecraft), in *Encyclopedia of Geomagnetism and Paleomagnetism,* eds Gubbins, D. & Herrero-Bervera, E., Springer, Dordrecht.

Cohen, Y. & Achache, J., 1990. New global vector magnetic anomaly maps derived from magsat data, *J. geophys. Res.,* **95**(B7), 10 783–10 800.

Cohen, Y. & Achache, J., 1994. Contribution of induced and remanent magnetisation to long-wavelength oceanic magnetic anomalies, *J. geophys. Res.,* **99,** 2943–2954.

Connerney, J.E.P., Acuna, M.H., Ness, N.F., Kletetschka, G., Mitchell, D.L., Lin R.P. & Reme, H., 2005. Tectonic implications of Mars crustal magnetism, *PNAS,* **102**(42), 14 970–14 975.

Connerney, J.E.P., 2009. Planetary magnetism, in *Planets and Moons,* Chapter 7, Volume 10, pp. 195–237, ed. Kono, M., Elsevier, Amsterdam, the Netherlands.

Constable, S. & Constable, C., 2004. Observing geomagnetic induction in magnetic satellite measurements and associated implications for mantle conductivity, *Geochem. Geophys. Geosyst.,* **5,** Q01006, doi:10.1029/2003GC000634.

Finlay, C.C. *et al.*, 2010. International Geomagnetic Reference Field: the eleventh generation, *Geophys. J. Int.,* **183**(3), 1216–1230, doi:10.1111/j.1365-246X.2010.04804.x.

Friis-Christensen, E., Lühr, H. & Hulot, G., 2006. Swarm: a constellation to study the Earth's magnetic field, *Earth Planets Space,* **58**(4), 351–358.

Grammatika, N. & Dyment, J., 1997. Anisotropy of the Magsat magnetic anomalies: real or fictitious? *International Association of Geomagnetism and Aeronomy General Assembly,* Uppsala, Abstract 4-15/08.

Hamoudi, M., Thébault, E., Lesur, V. & Mandea, M., 2007. GeoForschungsZentrum Anomaly Magnetic Map (GAMMA): a candidate model for the World Digital Magnetic Anomaly Map., *Geochem. Geophys. Geosyst.,* **8,** Q06023, doi:10.1029/2007GC001638.

Hemant, K. & Maus, S., 2003. A comparison of global lithospheric field models derived from satellite magnetic data, in *First CHAMP Mission Results for Gravity, Magnetic and Atmospheric Studies,* pp. 261–268, eds Reigber, C., Lühr, H. & Schwintzer P., Springer, Berlin.

Hemant, K., Thébault, E., Mandea, M., Ravat, D. & Maus, S., 2007. Magnetic anomaly map of the world: merging satellite, airborne, marine

and ground–based magnetic data sets, *Earth planet. Sci. Lett.,* **260**(1–2), 56–71.

Hood, L.L. & Zakharian, A., 2001. Mapping and modeling of magnetic anomalies in the northern polar region of Mars, *J. geophys. Res.,* **106**(E7), 14 601–14 619.

Hood, L.L., Zakharian, A., Halekas, J., Mitchell, D.L., Lin, R.P., Acuña, M.H., Binder, A.B., 2001. Initial mapping and interpretation of lunar crustal magnetic anomalies using Lunar Prospector magnetometer data, *J. geophys. Res.,* **106**(E11), 27 825–27 839.

Hulot, G., Olsen, N. & Sabaka, T.J., 2007. The present field, in *Geomagnetism, Treatise on Geophysics,* Vol. **5**, Elsevier, Amsterdam, pp. 33–72.

Korhonen, J. *et al.*, 2007. *Magnetic Anomaly Map of the World/Carte des Anomalies Magnétiques du Monde*, 1st edn., 1:50,000,000, CCGM/CCGMW, ISBN: 978-952-217-000-2.

Kuvshinov, A., Sabaka, T.J. & Olsen, N., 2006. 3-D electromagnetic induction studies using the Swarm constellation: mapping conductivity anomalies in the Earth's mantle, *Earth Planets Space,* **58,** 417–427.

Langel, R.A. & Estes R.H., 1985. Large-scale, near-field magnetic fields from external sources and the corresponding induced internal field., *J. geophys. Res.,* **90**(3), 2487–2494.

Langel, R.A. & Sweeney, R.A., 1971. Asymmetric ring current at twilight local time., *J. geophys. Res.,* **761,** 4420–4427.

Langel, R.A., Schnetzler, C.C., Phillips, J.D. & Horner, R.J., 1982. Initial vector magnetic anomaly map from MAGSAT. *Geophys. Res. Lett.,* **9,** 273–276.

Langel, R.A. & Hinze, W.J., 1998. *The Magnetic Field of the Earth's Lithosphere,* Cambridge University Press, Cambridge, pp. 429

Langlais, B., Purucker, M. & Mandea, M., 2004. Crustal magnetic field of Mars, *J. geophys. Res.,* **109,** E02008, doi:10.1029/2003JE002048.

Langlais, B., Lesur, V., Purucker, M.E., Connerney, J.E.P. & Mandea, M., 2009. Crustal magnetic field of terrestrial planets, *Space Sci. Rev,* doi:10.1007/s11214-009-9557-y. pp 27.

Lesur, V. & Maus, S., 2006. A global lithospheric magnetic field model with reduced noise level in the Polar Regions, *Geophys. Res. Lett.,* **33,** L13304, doi:10.1029/2006GL025826.

Lesur, V., Wardinski, I., Rother, M. & Mandea, M., 2008. GRIMM - The GFZ Reference Internal Magnetic Model based on vector satellite and observatory data, *Geophys. J. Int.,* **173,** 382–394.

Lesur, V., Wardinski, I., Hamoudi, M. & Rother, M., 2010. The second generation of the GFZ Reference Internal Magnetic Model: GRIMM-2, *Earth Planets Space,* **62**(10), 765–773.

Lillis, R.J., Purucker, M.E., Halekas, J.S., Louzada, K.L., Stewart-Mukhopadhyay, S.T., Manga, M. & Frey, H.V., 2010. Study of impact demagnetization at Mars using Monte Carlo modeling and multiple altitude data, *J. geophys. Res.,* **115,** E07007, doi:10.1029/2009JE003556.

Maus, S., Rother, M., Holme, R., Lühr, H., Olsen, N. & Haak, V., 2002. First scalar magnetic anomaly map from CHAMP satellite data indicates weak lithospheric field, *Geophys. Res. Lett.,* **29**(14), doi:10.1029/2001GL013685.

Maus, S. & Lühr, H., 2005. Signature of the quiet-time magnetospheric magnetic field and its electromagnetic induction in the rotating Earth, *Geophys. J. Int.,* **162,** 755–763, doi:10.1111/j.1365-246X.2005.02691.x.

Maus, S., Lühr, H. & Purucker, M., 2006. Simulation of the high-degree crustal field recovery for the Swarm constellation of satellites, *Earth Planets Space,* **58**(4), 397–407.

Maus, S., Sazonova, T., Hemant, K., Fairhead, J.D. & Ravat, D., 2007a. National Geophysical Data Center candidate for the World Digital Magnetic Anomaly Map, *Geochem. Geophys. Geosyst.,* **8,** Q06017, doi:10.1029/2007GC001643.

Maus, S., Lühr, H., Rother, M., Hemant, K., Balasis, G., Ritter, P. & Stolle, C., 2007b. Fifth-generation lithospheric magnetic field model from CHAMP satellite measurements, *Geochem. Geophys. Geosyst.,* **8,** Q05013, doi:10.1029/2006GC001521.

Maus, S. *et al.*, 2008. Resolution of direction of oceanic magnetic lineations by the sixth-generation lithospheric magnetic field model from CHAMP satellite magnetic measurements, *Geochem. Geophys. Geosyst.,* **9,** Q07021, doi:10.1029/2008GC001949.

Maus, S. *et al.*, 2009. EMAG2: a 2-arc min resolution Earth Magnetic Anomaly Grid compiled from satellite, airborne, and marine magnetic measurements. *Geochem. Geophys. Geosyst.,* **10,** Q08005, doi:10.1029/2009GC002471.

Neubert, T. *et al.*, 2001. Ørsted satellite captures high-precision geomagnetic field data., *EOS,* **82**(7), 81–88.

Ness, N.F., Behannon, K.W., Lepping, R.P., Whang, Y.C. & Shatten, K.H., 1974. Magnetic field observations at Mercury: preliminary results from Mariner 10, *Science,* **185**(4146), 151–160.

Olsen, N., 1999. Induction studies with satellite data, *Surv. Geophys.,* **20,** 309–340.

Olsen, N. *et al.*, 2006. The Swarm End-to-End mission simulator study: a demonstration of separating the various contributions to Earth's magnetic field using synthetic data, *Earth Planets Space,* **58**(4), 359–370.

Olsen, N., Glassmeier, K.-H. & Jia, X., 2010a. Separation of the magnetic field into external and internal parts, *Space Sci. Rev.,* **152,** 135–157, doi:10.1007/s11214-009-9563-0.

Olsen, N., Hulot, G. & Sabaka, T.J., 2010b. Sources of the geomagnetic field and the modern data that enable their investigation, in *Handbook of Geomathematics,* ch. 5, pp. 106–124, eds Freeden, W., Nashed, M.Z., Sonar, T., Springer-Verlag, Berlin, doi:10.1007/978-3-642-01546-5_5.

Olsen, N. & Kotsiaros, S., 2010. Magnetic satellite missions and data, in *Geomagnetic Observations and Models, IAGA Special Sopron Book Series,* Vol. 5, pp. 27–45, Springer-Verlag, Dordrecht, ISBN: 978-90-481-9857-3.

Olsen, N., Luhr, H., Sabaka, T.J., Michaelis, I., Rauberg, J. & Tøffner-Clausen, L., 2010. CHAOS-4—a high-resolution geomagnetic field model derived from low-altitude CHAMP data, AGU Fall Meeting, San Francisco, GP21A-0992.

Purucker, M.E., Sabaka, T.J., Langel, R.A. & Olsen, N., 1997. The missing dimension in Magsat and POGO anomaly studies, *Geophys. Res. Lett.,* **24**(22), 2909–2912.

Purucker, M.E. & Dyment, J., 2000. Satellite magnetic anomalies related to seafloor spreading in the South Atlantic Ocean, *Geophys. Res. Lett.,* **27**(17), 2765–2768.

Purucker, M.E. & Whaler, K., 2007. *Crustal Magnetism,* Treatise on Geophysics vol. 5: Geomagnetism, ch. 6, pp. 195–237, ed. Kono, M., Elsevier, Amsterdam, the Netherlands.

Purucker, M.E., Sabaka, T.J., Solomon, S.C., Anderson, B.J., Korth, H., Zuber, M.T. & Neumann, G.A., 2009. Mercury's internal magnetic field: constraints on large- and small-scale fields of crustal origin, *Earth planet. Sci. Lett.,* **285,** 340–346.

Purucker, M.E. & Nicholas, J.B., 2010. Global spherical harmonic models of the internal magnetic field of the Moon based on sequential and coestimation approaches, *J. geophys. Res.,* **115**(E12), E12007, doi:10.1029/2010JE003650.

Ravat, D., Langel, R.A., Purucker, M., Arkani-Hamed, J. & Alsdorf, D.E., 1995. Global vector and scalar Magsat magnetic anomaly maps, *J. geophys. Res.,* **100**(B10), 20 111–120 136.

Regan, R., Handschumacher, D. & Sugiura, M., 1981. A closer examination of the reduction of satellite magnetometer data for geological studies. *J. geophys. Res.,* **86**(B10), 9567–9573.

Reigber C., Lühr, H. & Schwintzer T., 2002. Champ, mission status. *Adv. Space Res.,* **30,** doi:10.1016/S02731177(02)00276-4.

Russell, C.T. & Dougherty, M.K., 2009. Magnetic fields of the outer planets, *Space Sci. Rev.,* **152**(1–4), 251–269, doi:10.1007/s11214-009-9621-7.

Sabaka, T.J., Olsen, N. & Purucker, M.E., 2004. Extending comprehensive models of the Earth's magnetic field with Ørsted and CHAMP data, *Geophys. J. Int.,* **159**(2), 521–547, doi:10.1111/j.1365-246X.2004.02421.x.

Sabaka, T.J. & Olsen, N., 2006. Enhancing comprehensive inversions using the Swarm constellation, *Earth Planets Space,* **58,** 371–395.

Schwarte J., Lühr, H. & Holme, R., 2003. Improved parameterization of external magnetic fields from CHAMP measurements, in *First CHAMP Mission Results for Gravity, Magnetic and Atmospheric Studies,* pp. 239–244, eds Reigber, C., Lühr, H., Schwintzer, P., Springer, Berlin.

Schott, J.J. & Thébault, E., 2010. Modelling the earth's magnetic field from global to regional scales, in *Geomagnetic Observations and Models,* IAGA Special Sopron Book Series vol. 5, pp. 229–265, Springer-Verlag, Heidelberg, ISBN: 978-90-481-9857-3.

Singh, B.P., Agarwal, A.K. & Rastogi, R.R., 1986. On the nature of residual trend in MAGSAT passes after removal of core and external components, *Ann. Geophys.,* **4B**(6), 653–658.

Solomon, S.C. *et al.*, 2008. Return to Mercury: a global perspective on MESSENGER's first Mercury flyby, *Science,* **321,** 59–62, doi:10.1126/science.1159706.

Sugiura, M., 1964. Hourly values of the equatorial Dst for the IGY, *Ann. IGY,* **35,** 9–45.

Thébault, E., 2006. Global crustal magnetic field modelling by successive regional anaysis, *Earth Planets Space,* **58,** 485–495.

Thébault, E., Purucker, M., Whaler, K., Langlais, B. & Sabaka, T.J., 2010. The magnetic field of the Earth's lithosphere, *Space Sci. Rev.,* **155**(1-4), 95–127, doi:10.1007/s11214-010-9667-6.

Thomson, A.W.P., Hamilton, B., Macmillan, S. & Reay, S.J., 2010. A novel weighting method for satellite magnetic data and a new global magnetic field model, *Geophys. J. Int.,* **181,** 250–260, doi:10.1111/j.1365-246X.2010.04510.x.

Trampert, J. & Snieder, R., 1996. Model estimations based on truncated expansions: possible artifacts in seismic tomography, *Science,* **271,** 1257–1260.

Tyler, R., Maus, S. & Lühr, H., 2003. Satellite observations of magnetic fields due to ocean tidal flow, *Science,* **299,** 239–241.

Uno, H., Johnson, C.L., Anderson, B.J., Korth, H. & Solomon, S.C., 2009. Modeling Mercury's internal magnetic field with smooth inversions, *Earth planet Sci. Lett.,* **285,** 328–339.

Wang, Z., 1987. Understanding models of the geomagnetic field by Fourier analysis, *J. Geomag. Geoelectr.,* **39,** 333–347.